Printed in the U.S.A.

Human Myosin Vc Is a Low Duty Ratio, Nonprocessive Molecular Motor*

Received for publication, November 7, 2007, and in revised form, January 2, 2008 Published, JBC Papers in Press, January 16, 2008, DOI 10.1074/jbc.M709150200

Yasuharu Takagi[‡], Yi Yang[‡], Ikuko Fujiwara[§], Damon Jacobs[¶], Richard E. Cheney[¶], James R. Sellers[‡1], and Mihály Kovács[‖2]

From the [‡]Laboratory of Molecular Physiology, NHLBI, National Institutes of Health, Bethesda, Maryland 20892-8015, [§]Laboratory of Cell Biology, NHLBI, National Institutes of Health, Bethesda, Maryland 20892-8017, [¶]Cell and Molecular Physiology, University of North Carolina School of Medicine, Chapel Hill, North Carolina 27599-7545, and the [‖]Department of Biochemistry, Eötvös University, H-1117 Budapest, Pázmány P. Sétány 1/C, Hungary

Myosin Vc is the product of one of the three genes of the class V myosin found in vertebrates. It is widely found in secretory and glandular tissues, with a possible involvement in transferrin trafficking. Transient and steady-state kinetic studies of human myosin Vc were performed using a truncated, single-headed construct. Steady-state actin-activated ATPase measurements revealed a V_{max} of 1.8 ± 0.3 s^{-1} and a K_{ATPase} of 43 ± 11 μM. Unlike previously studied vertebrate myosin Vs, the rate-limiting step in the actomyosin Vc ATPase pathway is the release of inorganic phosphate (~1.5 s^{-1}), rather than the ADP release step (~12.0–16.0 s^{-1}). Nevertheless, the ADP affinity of actomyosin Vc (K_d = 0.25 ± 0.02 μM) reflects a higher ADP affinity than seen in other myosin V isoforms. Using the measured kinetic rates, the calculated duty ratio of myosin Vc was ~10%, indicating that myosin Vc spends the majority of the actomyosin ATPase cycle in weak actin-binding states, unlike the other vertebrate myosin V isoforms. Consistent with this, a fluorescently labeled double-headed heavy meromyosin form showed no processive movements along actin filaments in a single molecule assay, but it did move actin filaments at a velocity of ~24 nm/s in ensemble assays. Kinetic simulations reveal that the high ADP affinity of actomyosin Vc may lead to elevations of the duty ratio of myosin Vc to as high as 64% under possible physiological ADP concentrations. This, in turn, may possibly imply a regulatory mechanism that may be sensitive to moderate changes in ADP concentration.

Class V myosins are part of the myosin superfamily, currently composed of as many as 37 types of myosins (1). This diverse superfamily is constituted with proteins that have been identified from conserved sequences in the catalytic domain (motor), which are needed for actin binding and ATP hydrolysis (2, 3). Within this actin-based molecular motor superfamily, class V myosins are one of the most ancient and widely distributed forms (4). Myosin Vs have been implicated in actin-dependent organelle transport (5, 6) and membrane trafficking (7, 8). In recent years, various studies using assorted scientific techniques, including both *in vitro* single molecule/ensemble biochemical and biophysical assays, as well as cell biological assays, have contributed to our current understanding of the mechanisms used by myosin V family members (9–11).

Within vertebrates, three genes of the class V myosin (Va, Vb, and Vc) have been discovered (12–14). Of these gene products, myosin Va (12, 15) has been the focus of attention. Myosin Va is expressed at high levels in neurons and melanocytes (5, 16–21). The lack of myosin Va in mouse can result in neurological seizures and critical defects in the transport of melanosomes (16, 22–24). Thus, studying this myosin at the molecular level may provide insights in human pathology. Myosin Vb is expressed in many tissue types, but Northern blot hybridization has shown that this protein is found primarily in the testes, kidney, liver, lung, and the heart (13). *In vivo* studies have shown that myosin Vb is associated with recycling of numerous receptors, including the transferrin receptor (25), muscarinic acetylcholine receptor (26), and the cystic fibrosis conductance regulator (27). Myosin Vc is expressed chiefly in epithelial cells in the pancreas, prostate, mammary, stomach, colon, and the lung (14). It has been suggested that one role of myosin Vc *in vivo* is membrane trafficking, specifically that of the transferrin receptor, where myosin Vb is also implicated. However, myosin Vc appears to be partially distinct with the same myosin Vb-associated membrane compartments (14).

The structure of myosin Va has been thoroughly studied (10, 12, 15, 28–30). Myosin Va is an oligomeric protein, which is composed of a dimerized heavy chain, each containing a motor domain, a lever arm containing six IQ motifs that bind a total of six light chains (mostly or entirely calmodulins) per heavy chain, followed by a coiled-coil region and a C-terminal globular tail. The sequence alignment of the three vertebrate myosin V isoforms showed that throughout the class there is ~50% amino acid identity. Myosin Vc, for example, shares ~62% identity to the myosin Va and Vb motor domains, ~20–30% identity in the coiled-coil region, and some differences in the globular tail region, such as the absence of the PEST site, found

* The costs of publication of this article were defrayed in part by the payment of page charges. This article must therefore be hereby marked "*advertisement*" in accordance with 18 U.S.C. Section 1734 solely to indicate this fact.

[1] Supported by funds from the intramural NHLBI program of the National Institutes of Health. To whom correspondence may be addressed: Laboratory of Molecular Physiology, NHLBI, Bldg. 50, Rm. 3523, National Institutes of Health, Bethesda, MD 20892-8015. Tel.: 301-496-6887; Fax: 301-402-542; E-mail: sellersj@mail.nih.gov.

[2] Supported by National Institutes of Health Research Grants D43 TW006230 and 1 R01 TW007241-01 funded by the Fogarty International Center and the NHLBI, National Institutes of Health, an EMBO-HHMI Startup Grant, and the Bolyai Fellowship of the Hungarian Academy of Sciences. To whom correspondence may be addressed: Dept. of Biochemistry, Eötvös University, H-1117 Budapest, Pázmány P. Sétány 1/C, Hungary. Tel.: 36-1-209-0555/8401; Fax: 36-1-381-2172; E-mail: stoci1@gmail.com.

in myosin Va and Vb (14). The structure of myosin Vb (31) and Vc has not been studied as thoroughly as myosin Va; however, the predicted structures from the amino acid sequence analysis exhibited that three isoforms are comparatively similar. The lack of the PEST domain for the myosin Vc reduces its size to ~12 kDa smaller than the other myosin Vs.

To characterize the molecular mechanism of these vertebrate myosin V isoforms, steady-state and transient solution kinetic studies have been performed using both myosin Va (32–38) and myosin Vb (31). The enzymatic properties of myosin Vc have not yet been characterized. Ensemble solution kinetics is a powerful technique that can be used to elucidate the fundamental kinetic properties of the different types of myosin, and a detailed kinetic analysis can furthermore be used to gain insights into the chemo-mechanical coupling of the molecular motor, as done for myosin Va (34, 35). One of the unique properties that distinguished the kinetic mechanism of myosin Va from the other previously studied myosins (2, 3, 39) is that it spends most of its kinetic cycle strongly bound to actin during steady-state ATPase cycling (>70%) and that the rate-limiting step of the actomyosin Va ATPase cycle is ADP release. These kinetic properties are consistent with this myosin being a *processive* motor, *i.e.* a protein that undergoes multiple enzymatic cycles while at least one of the motor domains of the molecule is attached to the filamentous actin, such that it can take multiple steps (40–43). The kinetic mechanism of myosin Vb has been studied (31) and showed indications that also this molecule is processive; however, direct observations that the dimerized form of this molecule is processive have not been shown. The kinetic mechanism of myosin Vc has not yet been studied in detail, and a detailed kinetic mechanism may be needed to understand its physiological function *in vivo*. Furthermore, the question whether myosin Vc isoform is processive or not would be of interest to unravel, because *Drosophila* myosin V was recently determined as a low duty ratio motor (*i.e.* a myosin head that spends only a small fraction of the catalytic cycle strongly bound to actin) that is presumably nonprocessive (44).

In this study, we report a full biochemical kinetic characterization of the *Homo sapiens* myosin Vc subfragment-1 (MVc-S1) protein. Steady-state and transient solution kinetic characterizations were performed using a recombinant single-headed MVc-S1 construct, bound with a single calmodulin. Additionally, to directly investigate if the recombinant form of the *H. sapiens* myosin Vc translocates actin in an *in vitro* actin gliding assay and, furthermore, in an attempt to visualize processive motion of single molecules of *H. sapiens* myosin Vc, a heavy meromyosin (HMM)[3] form of the double-headed construct, intact with six IQ motifs and an enhanced green fluorescent protein (eGFP) attached to each motor domain (eGFP-MVc-HMM) on the N-terminal end, was expressed and purified from the Sf9 baculovirus system. The biochemical kinetic characterization revealed that MVc-S1 is a low duty ratio motor, which spends most of its time during the actomyosin ATPase cycle residing in the states weakly bound to actin. Unlike the other two vertebrate myosins, Va and Vb, the kinetic cycle of myosin Vc is not rate-limited by its ADP release but by the inorganic phosphate (P_i) release, which is biochemically closer in resemblance to myosins that form ensemble structures to function in physiological conditions, such as skeletal muscle myosin II.

We conclude that myosin Vc is a nonprocessive motor protein and therefore employs a different mechano-chemical mechanism to perform its tasks in the cytoskeleton compared with both myosin Va and Vb. Acto-MVc has a relatively high ADP affinity, and this unusual kinetic difference may possibly make the mechanical activity sensitive to ADP concentration, *i.e.* the duty ratio of this motor may increase at even the moderate ADP concentrations in an *in vivo* environment, consistent with our kinetic simulation results, as well as reported for nonmuscle myosin IIB (45).

EXPERIMENTAL PROCEDURES

Expression and Purification of the Myosin Vc-S1 and HMM Proteins—Using a cDNA clone of the *H. sapiens* myosin Vc encoding the 2930 amino acids fused with an N-terminally fused enhanced GFP,[4] we engineered a cDNA fragment that encodes the first 777 amino acids, containing the motor domain plus the first predicted light chain binding IQ motifs (myosin Vc subfragment-1; MVc-S1). In addition to the subfragment-1-like construct, a heavy meromyosin-like myosin Vc construct with an N-terminally fused enhanced GFP (eGFP-MVc-HMM) was also engineered by encoding the first 1108 amino acids, containing the motor domain, the six predicted IQ motifs, and the predicted coiled-coil region. These amplified clones were subcloned into the pFastBac1 baculovirus transfer vector (Invitrogen) designed with a FLAG epitope tag (DYKDDDDK) fused C-terminally to aid in purification (46). Double-stranded DNA sequencing was performed to confirm the complete nucleotide sequencing from both engineered vectors.

Both constructs were coexpressed with *Xenopus* calmodulin in the Sf9 baculovirus system and purified essentially as described previously (46). (The amino acid sequence of *Xenopus* calmodulin is identical to that of the human protein.)

Actin and Reagents—Rabbit skeletal muscle actin was prepared as described previously (47). Pyrene iodoacetamide-labeled actin was prepared by labeling Cys-374 with pyrene iodoacetamide (Invitrogen) (48). Pyrene-labeled actin was depolymerized by dialysis against G-buffer (1 mM Tris (pH 8.0), 0.1 mM ATP, 0.1 mM $CaCl_2$, 0.5 mM dithiothreitol, and 1 mM NaN_3), centrifuged, and gel-filtered using a PD-10 column (Amersham Biosciences) to remove free dye. Actin concentration was determined using the extinction coefficient as follows: unlabeled actin, A_{290} = 26,600 M^{-1} cm^{-1} (49); pyrene-actin, A_{290}–A_{344} × 0.127/26,600 M^{-1} cm^{-1}; pyrene dye, A_{344} = 22,000 M^{-1} cm^{-1}.

Tetramethylrhodamine phalloidin (Invitrogen)-labeled filamentous actin and 10% biotinylated filamentous actin was prepared essentially as described by Ishijima *et al.* (50) and Takagi *et al.* (51). Labeled filaments lacking biotinylated globular actin

[3] The abbreviations used are: HMM, heavy meromyosin; TIRF, total internal reflection fluorescence; MANT-, 2′-(or-3′)-*O*-(*N*-methylanthraniloyl)-; MDCC, N-[2-(1-maleimidyl)-1ethyl]-7-(diethylamino)coumarin-3-carboxamide; MOPS, 3-(*N*-morpholino)propanesulfonic acid; PBP, phosphate-binding protein; eGFP, enhanced green fluorescent protein; MVc-S1, myosin Vc subfragment-1.

[4] D. Jacobs and R. E. Cheney, unpublished observations.

were used for the *in vitro* actin gliding assay, and biotinylated filaments only for the single molecule TIRF assays.

MANT-ATP and MANT-ADP were purchased from Molecular Probes (Invitrogen) and stored at −20 °C. MDCC-labeled, phosphate-binding protein (MDCC-PBP) (52) was generously provided by Dr. Howard D. White (Eastern Virginia Medical School, Norfolk, VA). All other reagents used in this study were from Sigma.

Steady-state ATPase Experiments—Steady-state ATPase measurements of myosin Vc, both in the presence and absence of filamentous actin, were measured using an NADH-coupled assay as described previously by Trentham *et al.* (53), De La Cruz *et al.* (35), and Wang *et al.* (54). The solutions used for these measurements included the following reagents: 10 mM MOPS (pH 7.2), 2 mM $MgCl_2$, 0.15 mM EGTA; 2 mM ATP and 50 mM KCl, 40 units/ml lactate dehydrogenase, 200 units/ml pyruvate kinase, 1 mM phosphoenolpyruvate, and 200 μM NADH. Changes in A_{340} were monitored using a Beckman DU640 spectrophotometer and stored for further data analysis.

Stopped-flow Experiments—All measurements were performed using an SF-2001 stopped-flow apparatus (KinTek Corp., Austin, TX) at 25 °C. For constancy, all stopped-flow experiments were performed using buffer (SF buffer) having the same contents. The SF buffer contained the following reagents: 20 mM MOPS (pH 7.0), 5 mM $MgCl_2$, 0.05 mM EGTA, and 50 mM KCl. To determine the kinetic parameters for P_i release, double-mixing stopped-flow experiments using MDCC-PBP (55) were performed as in Ref. 54. Only for the P_i release experiment was 10 mM KCl used. MVc-S1 and acto-MVc-S1 were preincubated with 0.02 units/ml of apyrase for at least 30 min at 25 °C to deplete any nucleotide in the sample when required. The optical setups of the apparatus are described in depth elsewhere (44, 54, 56). Post-mix concentrations of proteins and reagents are indicated throughout the text, unless stated otherwise.

Quenched-flow Experiments—Quenched-flow experiments were also performed at 25 °C in SF buffer. Quenched-flow experiments were performed using a KinTek RQF-3 apparatus as described previously (54) except that 1 M HCl was used as a quench.

Data Analysis—Data analyses of the steady-state and transient solution kinetic measurements were performed using either SigmaPlot 8.0 (Systat Software, San Jose, CA), OriginLab 7.5 (Microcal Corp. Northampton, MA), or the KinTek SF-2004 data analysis software. The means ± S.D. cited in this study are mostly averages of two to seven rounds of experiments performed using protein from different preparations.

In Vitro Actin Gliding Motility and Single Molecule TIRF Microscopy Assay—Both light microscopy assays were performed using an apparatus previously described by Sakamoto *et al.* (57, 62) with some minor modifications. Motility assays were performed in buffer containing the following reagents: 20 mM MOPS (pH 7.4), 5 mM $MgCl_2$, 0.1 mM EGTA, 50 mM KCl, 1 mM ATP, 5 μM calmodulin, 25 μg/ml glucose oxidase, 45 μg/ml catalase, 2.5 mg/ml glucose, and 20 mM dithiothreitol (final concentrations listed). Experiments were performed at 25 °C. Additionally, to determine whether ionic strength alters the motility of eGFP-MVc-HMM, single molecule motility assays were performed in the range varying from 0 to 250 mM KCl as shown previously for myosin Va (41). Observation chambers were also prepared from coverslips (Corning Inc., Corning. NY) using a protocol described previously (57). Data analysis of the *in vitro* actin gliding assay was performed using the ImageJ image analysis software (National Institutes of Health, Bethesda) with a data analysis algorithm described in Ref. 58 to track the leading ends of the labeled actin filaments.

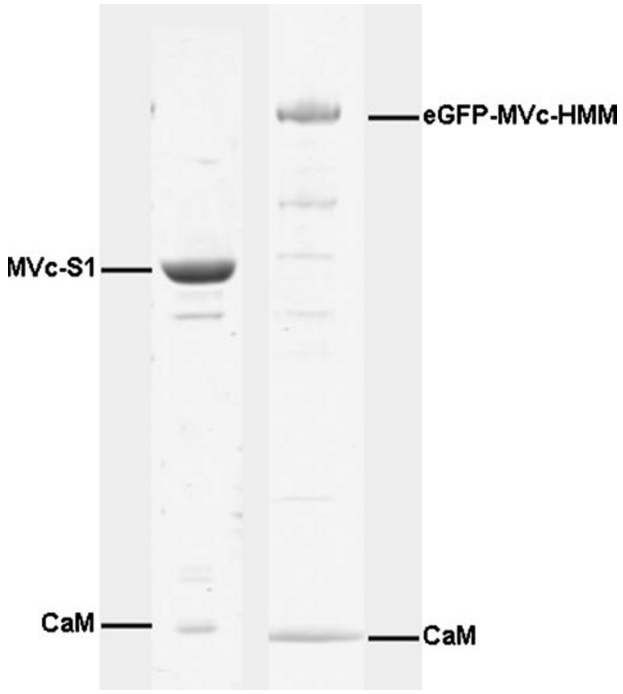

FIGURE 1. **SDS-PAGE of MVc-S1.** Samples were run on a 4–20% gradient SDS-polyacrylamide gel. *Lane 1*, FLAG affinity-purified MVc-S1 consisting of an 89.5-kDa heavy chain and a 15.7-kDa *Xenopus* calmodulin light chain (*CaM*). *Lane 2*, FLAG affinity-purified eGFP-MVc-HMM consisting of a 157.9-kDa heavy chain and a 15.7-kDa *Xenopus* calmodulin light chain.

Kinetic Simulation of the Actomyosin Vc ATPase Cycle—Kinetic simulations of the acto-MVc-S1 ATPase cycle were performed using Gepasi version 3.30 (Pedro Mendes, Virginia Bioinformatics Institute) based on Scheme 1 and the experimentally determined rate constants listed in Table 1.

RESULTS

Construct Design, Protein Expression, and Purification—Both the MVc-S1 and eGFP-MVc-HMM constructs were purified using FLAG affinity chromatography (Fig. 1). The single-headed subfragment-1 (S1) construct was used for the kinetic characterization, whereas the double-headed HMM construct was used to study its mechanical properties via *in vitro* actin gliding and single molecule TIRF assays. As described previously, the S1 construct only contained the motor domain and the first IQ motif, whereas the HMM construct contained the motor domain, the six (predicted) IQ-binding motifs, and the >200 amino acid stretch of the coiled-coil region to promote dimerization of the two heavy chains.

Protein expression was performed using the baculovirus expression system with the Sf9 insect cells, co-expressed with *Xenopus* calmodulin, at 27 °C using shaken cultures. Optimum expression of the protein was reached at ~3–3.5 days. Both

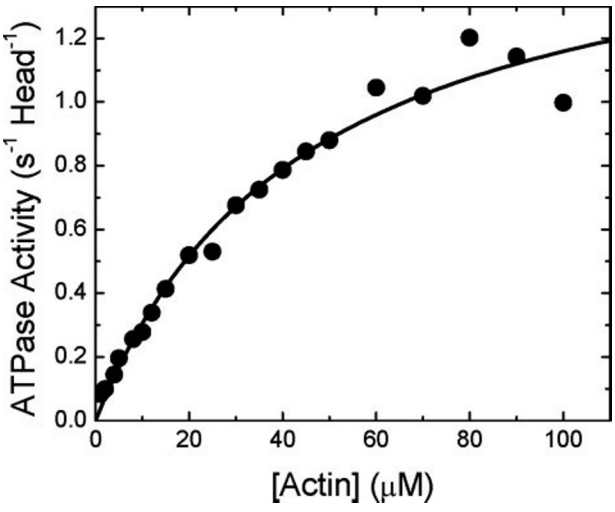

FIGURE 2. **Steady-state actin-activated ATPase activity of MVc-S1.** The ATPase activity of acto-MVc-S1 depended hyperbolically on actin concentration. This example data set shows a V_{max} of 1.7 ± 0.1 s^{-1} and a K_{ATPase} of 45.0 ± 6.8 μM. Average values taken from seven NADH-coupled assays from seven different protein purifications were as follows: 1.8 ± 0.3 s^{-1} (V_{max}) and half-maximal activation was achieved at 42.5 ± 10.6 μM (K_{ATPase}). The activity shown in the figure is expressed in terms of heads. Conditions: temperature = 25 °C; 10 mM MOPS (pH 7.0), 2 mM $MgCl_2$, 0.15 mM EGTA, 2 mM ATP, 50 mM KCl.

constructs showed reasonable levels of expression, generally yielding ~1 mg of protein purified from ~1 × 10^9 cells for the single-headed S1 construct, and ~0.5–0.7 mg of protein for the double-headed HMM construct.

Actin Activation of the Steady-state ATPase Activity—The steady-state ATPase activity of MVc-S1 was activated by actin to a maximal rate of 1.8 ± 0.3 s^{-1} (V_{max}), and half-maximal activation was achieved at 42.5 ± 10.6 μM (K_{ATPase}) (Fig. 2*A* and Table 1). Furthermore, in the absence of actin, the basal steady-state activity of MVc-S1 was 0.05 ± 0.01 s^{-1}. Association of MVc with actin therefore activates the steady-state activity of MVc-S1 by ~30-fold. Similarly to MVc-S1, steady-state ATPase activity of eGFP-MVc-HMM was activated by actin and yielded similar V_{max} and K_{ATPase} values (data not shown).

Association and Dissociation of MVc-S1 with Actin in the Absence of Nucleotide and in ADP—Pyrene-labeled filamentous actin has been used extensively to monitor the strong binding of myosin to actin in many myosins (59). Pyrene fluorescence is quenched on mixing of MVc-S1 or MVc-S1·ADP with pyrene-actin in the stopped flow, and the fluorescence decreases indicate the strong binding of MVc-S1 with pyrene-labeled actin. Fig. 3*A* shows the dependence of the k_{obs} (observed rate constant) of the observed fluorescence decreases on pyrene-actin concentration. The k_{obs} *versus* [pyrene-actin] plots were linear, and their slopes represent the second-order actin-binding rate constants of 0.66 ± 0.02 and 1.17 ± 0.03 $\mu M^{-1}\cdot s^{-1}$ in the absence of nucleotide (k_{-6}) and in ADP (k_{-10}), respectively.

The dissociation rates of MVc-S1 from pyrene-actin in the absence and presence of ADP were made using stopped-flow spectrophotometry chase experiments. The pyrene-acto-MVc-S1 rigor complex or the pyrene-acto-MVc-S1·ADP ternary complex was rapidly mixed with excess unlabeled filamentous actin in the stopped-flow apparatus. Pyrene fluorescence increases occur during dissociation of MVc-S1 or MVc-S1·ADP from the pyrene-actin, and the rebinding reaction is inhibited by the excess unlabeled filamentous actin. Single exponentials were fitted to the average transients, and the corresponding dissociation rate constants in the absence of nucleotide and in ADP were determined as 0.019 s^{-1} (k_6) and 0.051 s^{-1} (k_{10}), respectively.

The equilibrium constants in the absence (K_6) and presence of nucleotide (K_{10}) were also calculated using the determined second-order actin binding rate constants and the dissociation rate constants. The corresponding equilibrium constants in the absence of nucleotide and in ADP were determined as 0.029 μM (K_6) and 0.044 μM (K_{10}), respectively.

Interaction of ATP with Acto-MVc-S1—We measured the binding of ATP to acto-MVc-S1 by monitoring the ATP-induced dissociation of the pyrene-acto-MVc-S1 complex using the stopped-flow apparatus. Pyrene-acto-MVc-S1 (0.5 μM MVc-S1 and 1.0 μM pyrene-actin) incubated with apyrase was rapidly mixed with increasing concentrations of ATP (0–450 μM) under pseudo first-order conditions. Pyrene fluorescence increases after MVc-S1 dissociates from actin, and this fluorescence change can be fitted by a single exponential curve. k_{obs} increased hyperbolically with ATP concentration, approaching a maximal rate constant (k_1') of 287 s^{-1} with a half-maximum (K_1) at 288 μM ATP (K_1') (Fig. 4*A*). At low ATP concentrations, the data sets of the observed rate constants increased linearly with ATP concentration, and the apparent second-order rate constant ($K_1'k_1'$) was 0.75 ± 0.03 $\mu M^{-1}\cdot s^{-1}$ (Fig. 4*B*), for this particular example. $K_1'k_1'$ determined from the average of multiple experiments yielded an apparent second-order rate constant of 0.82 ± 0.03 $\mu M^{-1}\cdot s^{-1}$ (Table 1).

Interaction of ADP with Acto-MVc-S1—To determine the ADP dissociation rate constant from acto-MVc-S1 (k_5'), we monitored the decrease in fluorescence upon dissociation of MANT-ADP from acto-MVc-S1. 1 μM MVc-S1 was incubated with 20 μM filamentous actin and 50 μM MANT-ADP (pre-mix concentrations). This ternary complex was mixed rapidly with excess ATP (1 mM; pre-mix concentration). Upon mixing, the decrease in the MANT-ADP fluorescence was recorded, and the transients were fitted by single exponential curves. Fig. 5 shows an example of these averaged transients. The fits yielded rate constants of 15.6 ± 0.6 s^{-1} (= k_5').

To measure the ADP affinity of acto-MVc-S1, 1.0 μM pyrene-labeled actin was incubated with 0.5 μM MVc-S1 and various concentrations of ADP and then rapidly mixed with 150 μM ATP (pre-mixing concentrations). The transient of the pyrene fluorescence increases as the pyrene-actin dissociates from the MVc-S1. Fig. 6*A* shows an example of these transients, whereby pyrene-acto-MVc-S1 was incubated with 3 μM ADP (pre-mixing concentrations). The fluorescence increase was fitted by a double exponential, whereby the fast phase (~100 s^{-1}) corresponded to the ATP-induced dissociation of the ADP-free actomyosin complex, and the relative amplitude of this phase reports the fraction of acto-MVc-S1 free of bound nucleotide. The slower phase of the transient at low ADP concentrations, 15.8 ± 0.8 s^{-1}, reflects the kinetics of ADP dissociation from the actomyosin complex (k_5') (which must occur before ATP can bind and dissociate pyrene-acto-MVc-S1), and therefore the relative amplitude of this phase reports the fraction of acto-

TABLE 1

Kinetic parameters of the MVc-S1 ATPase cycle with corresponding values for myosins Va, Vb, and Drosophila myosin V

Numbering of the kinetic rates and equilibrium constants correspond to Scheme 1.

	Signal or calculation	Myosin Vc-S1[a]	Myosin Va[b]	Myosin Vb[c]	*Drosophila* myosin V[d]
Steady-state ATPase activity					
k_{basal} (s^{-1})	NADH assay	0.05 ± 0.01	0.03	0.09 ± 0.04	0.07 ± 0.013
V_{max} (s^{-1})	NADH assay	1.8 ± 0.3	15	9.7 ± 0.4	12.5 ± 0.8
K_{ATPase} (μM)	NADH assay	42.5 ± 10.6	1.4	28.1 ± 5.9	9.9 ± 0.6
Actin binding					
k_{-6} (μM^{-1} s^{-1})	Pyrene-actin	0.66 ± 0.02	73		2.5 ± 0.29
k_6 (s^{-1})	Pyrene-actin	0.019	0.0036		0.04 ± 0.001
K_6 (μM)	k_6/k_{-6}	0.029	4.9×10^{-6}		0.016
k_{-10} (μM^{-1} s^{-1})	Pyrene-actin	1.17 ± 0.03	4.2		2.3 ± 0.14
k_{10} (s^{-1})	Pyrene-actin	0.051	0.032		0.43 ± 0.01
K_{10} (μM)	k_{10}/k_{-10}	0.044	0.0076		0.19
K_9 (μM)	MDCC-PBP	14	9 ± 2[e]		70 ± 10
ATP binding					
$K_1'k_2'$ (μM^{-1} s^{-1})	Pyrene-actin	0.82 ± 0.03	0.9		0.36 ± 0.006
	MANT-ATP			0.31 ± 0.02	
k_2' (s^{-1})	Pyrene-actin	287	771 ± 70[e]		>180
	Tryptophan		≥750		
ATP hydrolysis					
$k_3 + k_{-3}$ (s^{-1})	Quenched-flow	90			
	Tryptophan		750		68 ± 4.7
	MDCC-PBP		>250		
K_3	Quenched-flow calculation	0.54			
	Quenched-flow		5.3		0.39 ± 0.22
P_i release					
k_4 (s^{-1})	MDCC-PBP	0.16			
	$k_{basal}(1+K_3)/K_3$		0.03		
k_4' (s^{-1})	MDCC-PBP	1.5	110 ± 10[e]		177 ± 18
k_4'/K_9 (μM^{-1} s^{-1})	MDCC-PBP (calculated)	0.11	12		
ADP binding					
k_5' (s^{-1})	MANT-ADP chase	15.6 ± 0.6	12	11.1 ± 2.1	150
	Pyrene-actin	15.8 ± 0.8			
	Pyrene-actin (simulated)		16		
K_5' (μM)	Pyrene-actin	0.25 ± 0.02			
	MANT-ADP amplitude				
	k_5'/k_{-5}' (MANT-ADP data)		0.8		
k_{-5}' (μM^{-1} s^{-1})	k_5'/K_5' (calculated)	~56–72			
k_{-5} (μM^{-1} s^{-1})	MANT-ADP		4.6		2.2 ± 0.3
Actin-ADP coupling					
K_{10}/K_6	Pyrene-actin (calculated)	~1.5	~1550		~4.8

[a] Data refer to this study.
[b] Data refer to Ref. 34 unless otherwise stated.
[c] Data refer to Ref. 31.
[d] Data refer to Ref. 44.
[e] Data refer to Ref. 38.

MVc-S1 bound with ADP. This ADP dissociation rate constant determined from the pyrene-actin fluorescence signal agrees well with the MANT-ADP fluorescence decrease upon dissociation from the acto-MVc-S1 (15.6 ± 0.6 s^{-1}) (Fig. 5 and Table 1).

A hyperbolic fit to the plot of the percent amplitudes of the slow phase (*i.e.* 100% × (A_{slow}/(A_{slow} + A_{fast}))) *versus* ADP concentration allowed for the determination of the acto-MVc-S1 ADP dissociation constant (K_5') of 0.25 ± 0.02 μM (Fig. 6*B* and Table 1). Thus, the ADP affinity of MVc-S1, in the presence of actin, is high, ~3-fold greater than that of chicken myosin Va (34).

Transient Kinetics of ATP Hydrolysis by MVc-S1—The ATP hydrolysis kinetics of MVc-S1 was measured using the quenched flow technique. MVc-S1 or acto-MVc-S1 was rapidly mixed with [γ-^{32}P]ATP, and the time course of P_i liberation was monitored over time. When MVc-S1 was mixed with ATP in single turnover conditions (1.5 μM protein and 1.5 μM nucleotide post-mix), the time course of the reaction consisted of two phases (Fig. 7*A*). The first phase had an amplitude of 0.49 μM P_i (corresponding to a fractional amplitude of 0.34) and a k_{obs} of 1.1 s^{-1}, which is likely limited by ATP binding. The slower second phase had a k_{obs} of 0.083 s^{-1}, in agreement with the basal steady-state activity of MVc-S1 (measured as 0.062 s^{-1} under the same reactant conditions in the NADH-linked assay).

When mixed with excess ATP in the quenched flow, MVc-S1 produced a P_i burst with an amplitude of 0.40 mol of P_i/mol of MVc-S1 (Fig. 7*B*). The burst was followed by a linear steady-state phase of P_i production characterized by a turnover rate of 0.064 s^{-1}, again in agreement with the results of the above quenched flow and steady-state measurements. When the same experiment was performed in the presence of 15 μM actin (post-mix), the steady-state rate was accelerated to 5-fold to 0.32 s^{-1} (in line with NADH-linked steady-state ATPase measurements (Fig. 2)), but the burst amplitude was not markedly affected (0.35 mol of P_i/mol of MVc-S1) (Fig. 7*C*). Using these burst amplitudes (B), the hydrolysis equilibrium constant (K_3) can be estimated by the following equation: $B = K_3/(1 + K_3)$; K_3 therefore is ~0.54. ATP hydrolysis for MVc-S1 is therefore reversible.

By following the time course of the reaction until near-complete exhaustion of ATP, we detected signs of weak product

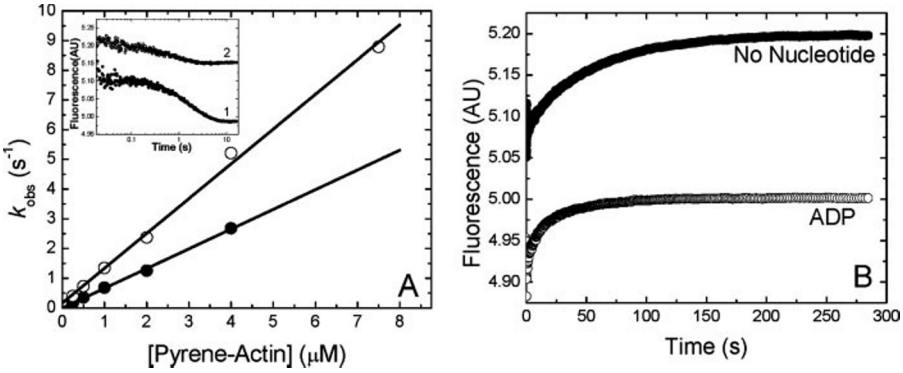

FIGURE 3. **Interaction of MVc-S1 with actin in the absence of nucleotide and in the presence of ADP.** *A*, dependence of the k_{obs} values of the recorded pyrene fluorescence transients via mixing 0.3 μM MVc-S1 with various pyrene-actin concentrations (0.25–7.5 μM; post-mix concentration) as indicated. Transients were recorded in the absence of any nucleotide (*solid symbols*) and in the presence of 20 μM ADP (*open symbols*). The second-order binding rate constants were determined by fitting a linear curve to the k_{obs} values, which yielded the second-order binding rate constants, 0.66 ± 0.02 $\mu M^{-1}\cdot s^{-1}$ (k_{-6}) and 1.17 ± 0.03 $\mu M^{-1}\cdot s^{-1}$ (k_{-10}) in the absence of nucleotide and in ADP, respectively. *Inset* shows an example of pyrene fluorescence transients recorded at 1 μM pyrene-actin (*trace 1*, *solid symbols*, no nucleotide trace, $k_{obs} = 0.68\ s^{-1}$; *trace 2*, *open symbols*, in ADP trace, $k_{obs} = 1.34\ s^{-1}$). Traces were offset for clarity. The transients were fitted using a single exponential curve fit. *B*, pyrene fluorescence transients to determine dissociation rates of MVc-S1 from pyrene-actin, both in the absence of nucleotide and in ADP. Chase experiments where a pre-mixture of the pyrene-acto-MVc-S1 rigor complex or the pyrene-acto-MVc-S1·ADP ternary complex (0.3 μM MVc-S1 and 0.5 μM pyrene-actin, in the absence of nucleotide (*solid symbols*) or 20 μM ADP (*solid symbols*)) were rapidly mixed with excess unlabeled 20 μM actin in the stopped-flow apparatus. Averaged transients were fitted to a single exponential curve. Corresponding dissociation rates in the absence of nucleotide and 20 μM ADP were 0.019 and 0.051 s^{-1}, respectively.

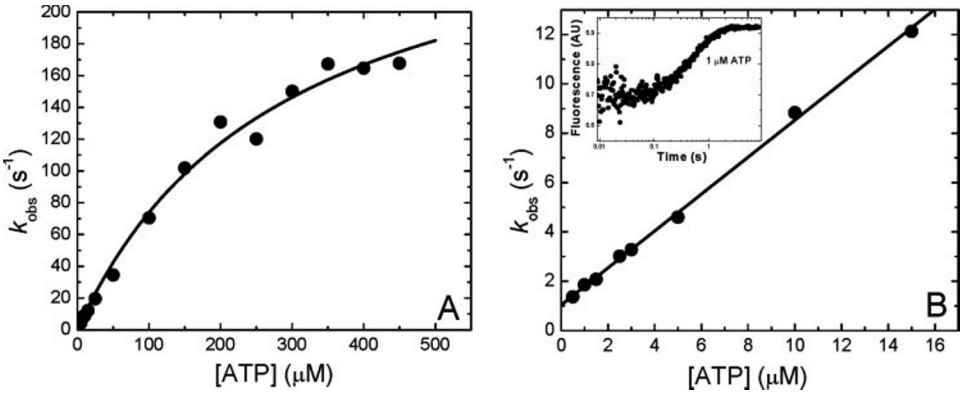

FIGURE 4. **Interaction of ATP with acto-MVc-S1.** *A*, binding of ATP to pyrene-acto-MVc-S1 was monitored to observe the ATP-induced dissociation of the pyrene-actomyosin complex. A preincubated pyrene-acto-MVc-S1 complex (0.5 μM MVc-S1 and 1.0 μM pyrene-actin) was mixed with increasing concentrations of ATP (0–450 μM). Pyrene fluorescence increase was observed because of MVc-S1 dissociation from actin. Fluorescence transients were fitted to single exponential curves. The k_{obs} increased with increasing ATP concentration. The maximal observed rate constant was $k_1' = 287\ s^{-1}$ with a half-saturation (K_1) at 288 μM ATP. At low [ATP], k_{obs} grew linearly with ATP concentration. A linear fit at low [ATP] yielded an apparent second-rate constant, $K_1'k_2' = 0.75\ \mu M^{-1}\cdot s^{-1}$. *B*, same data as *A*, but graph only shows data at low ATP concentrations (0.5–15 μM). A linear curve fit to the plot of k_{obs} *versus* [ATP] gave an apparent second-order rate constant of 1.20 ± 0.01 $\mu M^{-1}\cdot s^{-1}$. *Inset* shows an example of a pyrene-actin fluorescence transient recorded at 1 μM ATP ($k_{obs} = 1.86\ s^{-1}$).

inhibition by ADP (Fig. 7*C*). As expected from the kinetic parameters in Table 1, the ADP inhibition was much less pronounced in acto-MVc-S1 than in acto-MVa-S1, where ADP release is rate-limiting (34, 35).

Kinetics of the P_i Release Step—We monitored the time course of P_i release from MVc-S1·ADP·P_i and acto-MVc-S1·ADP·P_i using MDCC-PBP, a fluorescently labeled P_i-binding protein (55, 60). In double-mixing stopped-flow experiments, MVc-S1 was first mixed with ATP under single turnover conditions (5.2 μM MVc-S1 and 4 μM ATP after the first mix), incubated for 3 s so that ATP binding and hydrolysis can occur, and then rapidly mixed with actin (0–17.5 μM after the second mix) to monitor basal and actin-activated P_i release. Time courses of P_i release were best fit with single exponentials. Fig. 8*A* shows examples of transients, including their curve fits. The fitted k_{obs} values depended hyperbolically on actin concentration, starting from 0.16 s^{-1} in the absence of actin (k_4) and delineating a maximal P_i release rate constant of 1.5 s^{-1} (k_4') reaching half-saturation at 14 μM actin (K_9) (Fig. 8*B*).

In Vitro Actin Gliding Assay—*In vitro* actin gliding assays were performed to measure the velocity (v) at which the eGFP-MVc-HMM translocates tetramethylrhodamine-phalloidin-labeled filamentous actin filaments using a TIRF microscope setup equipped with a shutter to illuminate the field briefly every 10 or 20 s, to minimize photobleaching of the labeled actin filaments. Actin filaments more than 5 μm in length were tracked for more than 3 min. Time-lapse images were collected digitally and analysis of the leading edge of the actin filaments in the direction of translocation was performed by tracking the actin filaments over sequential images using the ImageJ image analysis software. The velocity distribution of actin filaments gliding over eGFP-MVc-HMM at saturating ATP concentration (1 mM) was 24.1 ± 7.8 nm·s^{-1} (means ± S.D.) (Fig. 9). A Gaussian fit to the velocity distribution histogram was used to determine the means ± S.D.

Single Molecule Motility Assay—Single molecule TIRF microscopy assay (43) was performed as reported previously from our laboratory (61, 62). The single molecule TIRF microscopy assay is a direct indication of whether or not the myosin is processive *in vitro*. TIRF microscopy experiments were performed using the recombinant heavy meromyosin-like myosin Vc construct encoding the first 1108 amino acids, containing the motor domain, the six predicted IQ motifs, and the coiled-coil region with an N-terminally fused enhanced GFP (eGFP-MVc-HMM). The assay was performed over a range of KCl concentrations (0–300 mM) to determine whether KCl affects the single molecule processivity of eGFP-MVc-HMM, as reported previously for myosin Va (41). The images recorded did not show any processive motion of the eGFP-MVc-HMM over the range of KCl or ATP concentrations (1 μM to 1 mM)

whereby the experiments were performed (data not shown), even though the eGFP-MVc-HMM does bind to and detach from actin filaments. This nonprocessive behavior is expected of single molecules of eGFP-MVc-HMM from the transient kinetic rates, *i.e.* specifically the P_i release limitation of the ATPase cycle, determined using the MVc-S1 in this study. We conclude that the recombinant double-headed myosin Vc construct, eGFP-MVc-HMM, under unloaded *in vitro* conditions, is not processive as a single molecule.

Kinetic Simulations—Kinetic simulations of the acto-MVc-S1 ATPase cycle were performed based on Scheme 1 and the experimentally determined rate constants listed in Table 1. Steps K_1, K_1, and K_7 (ATP binding to M5c-S1 detached from actin) were omitted from the simulations, because their parameters are unknown and the flux through these steps is negligible. Parameters used in the simulations but not listed in Table 1 were as follows: $k_9 = 1400\ s^{-1}$, $k_{-9} = 100\ \mu M^{-1}\ s^{-1}$ (to yield a rapid step with the measured $K_9 = 14\ \mu M$); $k_3 = 31.6\ s^{-1}$, $k_{-3} = 58.4\ s^{-1}$ (calculated from K_3 and $(k_3 + k_{-3})$ in Table 1); $k_5' = 14.7\ s^{-1}$ (average of k_5' values listed in Table 1); $k_{-5}' = 64\ \mu M^{-1}\ s^{-1}$.

First, we performed a global fit of the mechanism to attain the measured actin concentration dependence of the steady-state ATPase activity. In this fit, we floated the parameters of the experimentally inaccessible steps K_8 and K_3' as well as the k_4' rate constant, which might not precisely equal the maximal observed P_i release rate constant of the MDCC-PBP measurements (Fig. 7).

The [actin] dependence of the partitioning between the weak binding MVc·ATP, MVc·ADP·P_i, and acto-MVc·ADP·P_i states (and acto-MVc·ATP, if relevant) is dictated by the reversible K_3 and K_9 equilibria, with possible contributions from K_8 and/or K_3'. The fact that $K_9 \times (1 + K_3)/K_3$ (= 40 μM) nearly equals K_{ATPase} (= 42.5 μM) caused the fits to produce nearly complete dissociation of MT from actin following ATP binding (*i.e.* in the well fitting models K_8 was ≥1 mM). The presence or absence of actin-attached hydrolysis (K_3') did not affect the outcome of the steady-state parameters (ATPase activity and duty ratio) at the experimentally applied actin concentrations. Therefore, in further simulations we used two extremes of the adequately fitting parameter sets to calculate the dependence of the ATPase activity and the duty ratio on actin and ADP concentration. Importantly, these two sets of parameters (see Fig. 10, *A* and *B*) yielded similar ATPase activity and duty ratio values because of the same maximal effective rate of P_i release from acto-MVc (around 1.5 s^{-1}). Set 1 represented a mechanism in which actin-attached ATP hydrolysis does not occur ($k_3' = 0$, $k_{-3}' = 0$, $K_8 = 1$ mM (rapid step), $k_4' = 1.618\ s^{-1}$), whereas set 2 contained a rapid and favorable actin-attached ATP hydrolysis step ($k_3' = 100\ s^{-1}$, $k_{-3}' = 3\ s^{-1}$, $K_8 = 1$ mM (rapid step), $k_4' = 1.508\ s^{-1}$). In both conditions, the duty ratio of MVc-S1 depended hyperbolically on actin concentration, yielding a maximum value of 0.095 (reaching half-saturation at 31 μM actin) in the absence of background ADP ([ATP] = 1 mM, [ADP] = 0, [actin] scanned between 0 and 100 μM; Fig. 10*A*). At saturating actin concentration (using set 1), the increase of background [ADP] from 0 to 200 μM caused the ATPase activity of MVc to decrease to 39% of its original value (from 1.34 to 0.53 s^{-1}), whereas the duty ratio increased nearly 7-fold (from 0.093 to 0.64) ([actin] = 1 mM, [ATP] = 1 mM, [ADP] scanned between 0 and 200 μM; Fig. 10*B*).

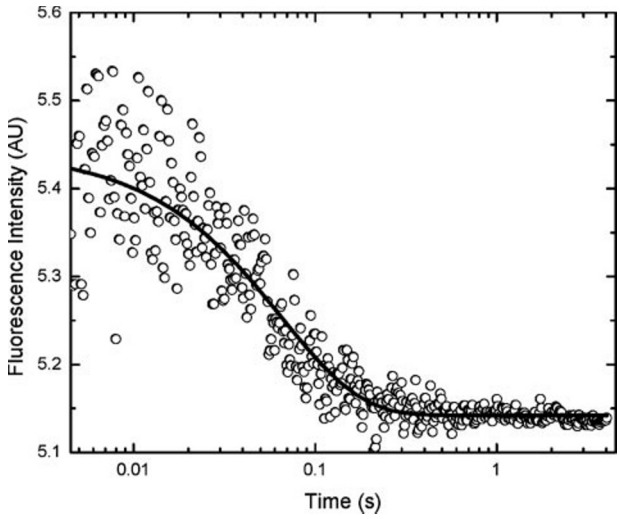

FIGURE 5. **MANT-ADP release from acto-MVc-S1.** Average time course of the MANT-ADP fluorescence decrease as MANT-ADP was displaced from MVc-S1. Initially, 50 μM MANT-ADP, 1 μM MVc-S1, and 20 μM filamentous actin were mixed, and this mixture was subsequently mixed with 1 mM ATP (pre-mixing concentrations). The *solid line* is the best single exponential fit, whereby the observed rate constant (k_5') was 16.0 ± 0.6 s^{-1}.

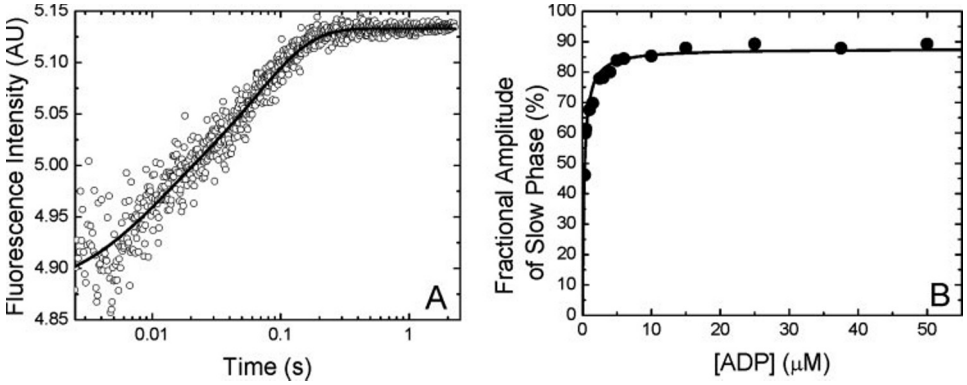

FIGURE 6. **Acto-MVc-S1 ADP affinity.** *A*, 1.0 μM pyrene-labeled actin was initially incubated with 0.5 μM MVc-S1 and various concentrations of ADP. This preincubated mixture was then mixed with 150 μM ATP (pre-mixing concentrations). Shown is an averaged time course of the pyrene fluorescence increase because of dissociation of the MVc-S1 from the pyrene-labeled actin. In this particular example, 3 μM ADP was used in the preincubated mixture. *Solid line* is the best double exponential fit to the data. The observed rate constant of the slow phase (k_5') in this case was 15.1 ± 0.6 s^{-1}. *B*, shown is the ADP dependence of the relative amplitude of the slower phase of the double exponential fit to the averaged time course of the pyrene fluorescence increase (*i.e.* 100% × ($A_{slow}/(A_{slow} + A_{fast})$)). Fitting the data with a quadratic equation yielded a K_d value 0.25 ± 0.02 μM (=K_5').

DISCUSSION

The kinetic characterization of the MVc-S1 and the *in vitro* motility assays performed using the eGFP-MVc-HMM revealed that the biochemistry of the vertebrate myosin Vc actomyosin ATPase cycle is fun-

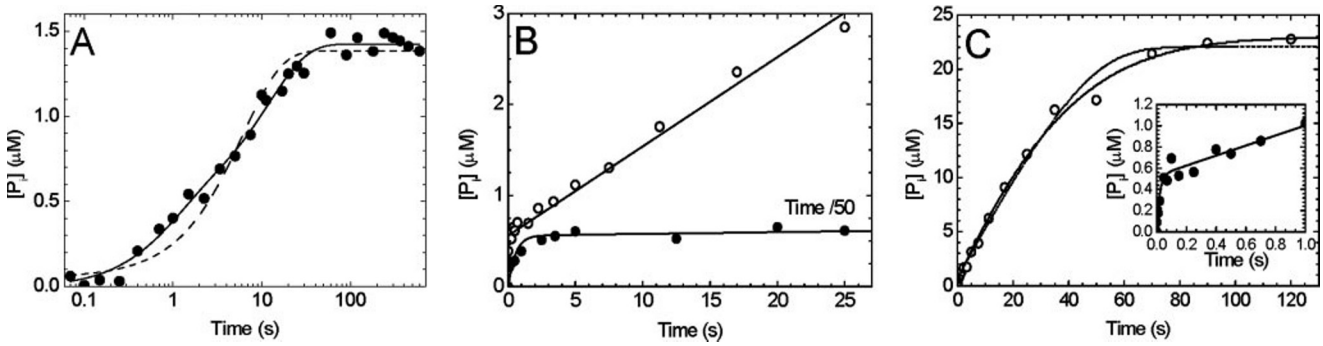

FIGURE 7. **Transient kinetics of ATP hydrolysis by MVc-S1 monitored by quenched flow.** *A*, time course of P_i liberation upon rapidly mixing 1.5 μM MVc-S1 with 1.5 μM [γ-^{32}P]ATP. The *solid line* indicates the best double exponential fit to the data with rate constants of 1.1 s^{-1} (fractional amplitude 0.34) and 0.083 s^{-1}. The best single exponential fit (*dashed line*) showed systematic deviation from the data points. *B* and *C*, P_i liberation upon mixing 1.5 μM MVc-S1 with 25 μM [γ-^{32}P]ATP, in the absence (*B*) and presence (*C*) of 15 μM actin. *B*, in the absence of actin, an exponential burst phase having an amplitude of 0.59 μM P_i (corresponding to 0.40 mol of P_i/mol of MVc-S1) and a rate constant of 90 s^{-1} was followed by a linear steady-state phase indicating a turnover rate of 0.064 s^{-1}. *Open symbols* show all the data obtained in this experiment. *Closed symbols* show the initial phase (*i.e.* time/50) of the data. *C*, similar burst phase was observed in the presence of 15 μM actin (amplitude, 0.35 mol of P_i/mol of MVc-S1, k_{obs} = 50 s^{-1}), but the steady-state turnover rate was accelerated to 0.32 s^{-1}. The time course of ATP hydrolysis was followed until quasi-complete exhaustion of the substrate to monitor product inhibition by ADP. The *solid line* in the *main panel* is a simulated progress curve of P_i liberation resulting from a global fitting procedure using the kinetic parameters of Table 1 and leaving the ADP binding rate constant of actomyosin (k_{-5}') as a floating parameter. The best fit was obtained at k_{-5}' = 18 $\mu M^{-1}\cdot s^{-1}$. The *dashed line* is a progress curve with a fixed k_{-5}' = 5 $\mu M^{-1}\cdot s^{-1}$. *Inset* shows the data points from the initial period (*i.e.* time 0–1 s) of this burst phase with the fit.

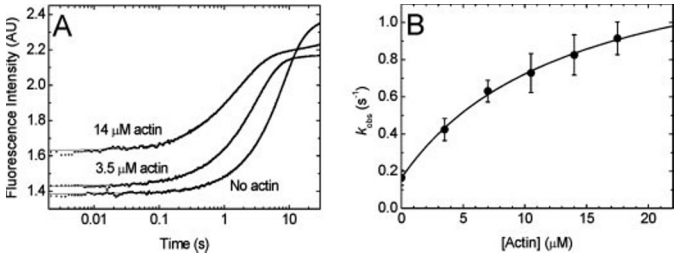

FIGURE 8. **P_i release from MVc-S1 and acto-MVc-S1 monitored by MDCC-PBP fluorescence.** *A*, MDCC-PBP fluorescence traces obtained in double-mixing stopped-flow experiments where MVc-S1 was first mixed with ATP (5.2 μM MVc-S1 and 4 μM ATP after the first mix), aged for 3 s, and then rapidly mixed with different concentrations of actin (as indicated). Single exponential fits to the traces are shown (k_{obs} = 0.082 s^{-1} (no actin), 0.34 s^{-1} (3.5 μM actin post-mix concentration), 0.67 s^{-1} (14 μM actin post-mix concentration)). *B*, dependence of the k_{obs} values on actin concentration. The best hyperbolic fit to the data yielded a maximum of 1.5 s^{-1}, with half-saturation at 14 μM actin and a *y* intercept of 0.16 s^{-1}.

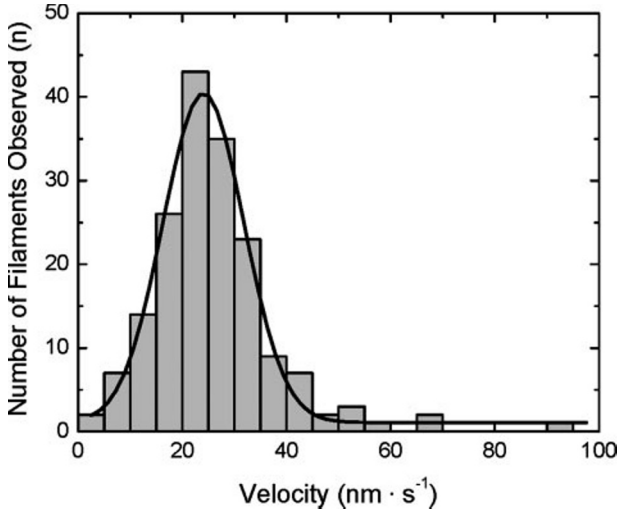

FIGURE 9. ***In vitro* actin gliding assay of eGFP-MVc-HMM.** Actin gliding velocity (*v*) distribution of eGFP-MVc-HMM in 1 mM ATP (v = 24.1 ± 7.8 nm·s^{-1}, n = 175). Actin gliding assays were performed in the following conditions: Buffer: 20 mM MOPS (pH 7.4), 5 mM $MgCl_2$, 0.1 mM EGTA, 50 mM KCl, 1 mM ATP, 5 μM calmodulin, 25 μg/ml glucose oxidase, 45 μg/ml catalase, 2.5 mg/ml glucose, and 20 mM dithiothreitol (final concentrations listed). Temperature = 25 °C.

damentally different from the other vertebrate myosin V isoforms, as well as the invertebrate *Drosophila* myosin V. We discuss these differences and the implications of these unique characteristics of myosin Vc.

Hum-MVc-S1 Exhibits a Low Duty Ratio—Kinetic analysis of MVc-S1 demonstrated that the rate-limiting step in the acto-MVc-S1 ATPase cycle is the P_i release step (k_4' = 1.5 s^{-1}), which is close to the maximal steady-state ATPase rate (V_{max} = 1.8 ± 0.3 s^{-1}) and ~10 times slower than the ADP release rate. The rate limitation of myosin Vc by the P_i release step in the actomyosin ATPase cycle contrasts to other vertebrate myosin Vs (Va and Vb) whose ADP dissociation rate constant (k_5') is rate-limiting (31, 34, 36). It has been shown that the rate-limiting P_i release is a common feature of ensemble myosins such as skeletal muscle myosin II (63), non-muscle myosin IIA (45), and some myosin Is (59, 64, 65). The duty ratios of ensemble myosins are generally known to be small (*i.e.* ≤10%).

By assuming a very simplified cycle in which only two states alternate, a strong and a weak actin-binding one, which the ADP release rate constant (k_5' = 12–16 s^{-1}) is the exit rate from the strong binding state and the P_i release rate constant (k_4' = 1.5 s^{-1}) is the exit rate from the weak binding state, we can estimate the duty ratio of MVc-S1 by using the equation $k_4'/(k_4' + k_5')$ (34, 39). This yields a duty ratio within the range of 6–13% for MVc-S1, which is dramatically lower compared with some other high duty ratio motors such as myosin Va and VI (34, 66) but quite comparable with the low duty ratio myosins as mentioned.

To calculate the duty ratio under different conditions, we performed global kinetic simulations using the parameters determined from the biochemically observed rates in this study. The simulations generated a duty ratio in line with the above simple calculations (around 10%), and an increase of this duty ratio by ~7-fold to more than 60% in the presence of moderate background levels of [ADP] (Fig. 10). Simulations were performed for ADP concentrations from 0 to 200 μM, which has

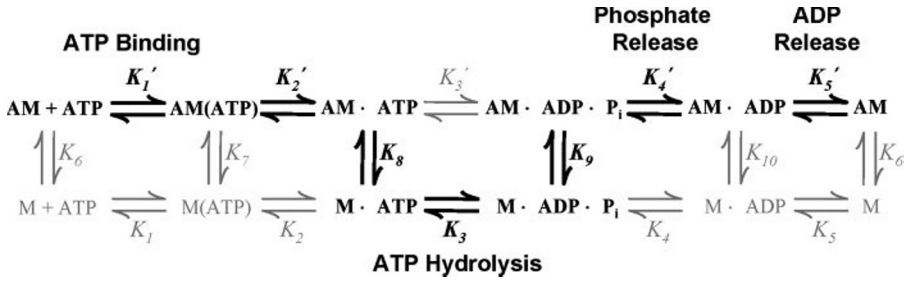

SCHEME 1. **Actomyosin ATPase cycle.** The abbreviations used are as follows: *A*, actin; *M*, myosin; Equilibrium constants (K_n and K_n') are expressed in rightward and downward directions as shown. *Arrows* representing associations and dissociations of ligands are excluded. For simplicity, the main flux pathway of the actomyosin ATPase reaction is highlighted in *bold* and with a *darker font color*.

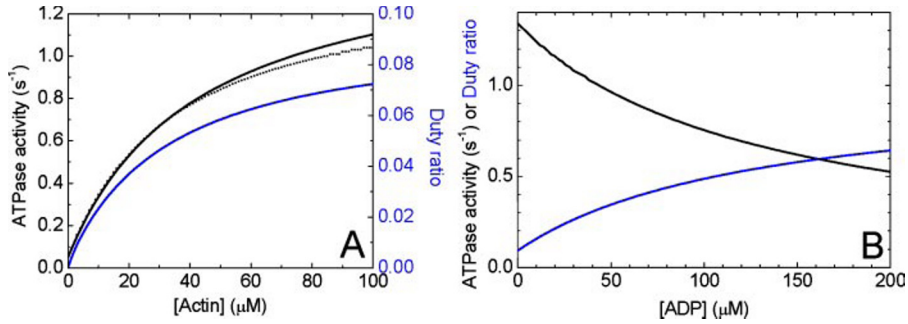

FIGURE 10. **Dependence of steady-state parameters (ATPase activity, duty ratio) of MVc-S1 on actin (*A*) and background ADP concentration (*B*).** *A*, dependence of the ATPase activity *(left axis*; *solid black line*: target for global fit (V_{max} = 1.5 s^{-1}, K_{ATPase} = 43.5 μM); *black dots,* best fit simulation) and duty ratio (*right axis*; *blue line*) of MVc-S1 on actin concentration in the absence of ADP background. Parameter sets 1 and 2 described in the text yielded similar ATPase and duty ratio values. *B*, dependence of the ATPase activity (*black*) and duty ratio (*blue*) of MVc-S1 at saturating [actin] (1 mM) on ADP concentration. Parameter set 1 was used in *B*. ATP concentration was kept constant at 1 mM in all simulations.

been suggested as physiological concentrations, for example in muscle at rest and during work (67–69). This increase in duty ratio because of increased [ADP] may be a regulatory mechanism *in vivo* to modulate the intracellular function of myosin Vc in the cell, perhaps as a tension generating, or anchoring, myosin.

Furthermore, the estimated low duty ratio of the MVc-S1 is consistent with our observations that single molecules of eGFP-MVc-HMM exhibit nonprocessive movements in the single molecule TIRF microscopy assays. Thus, the biochemical rates obtained from the steady-state and transient kinetic solution experiments provided a satisfactory basis for its mechanochemical behavior.

Biochemical and Mechanical Implications of Human Myosin Vc as a Cytoskeletal Cargo Transporter—The duty ratio, discussed above, captures the essence of how different myosin Vc is compared with myosins Va and Vb. However, a number of unique details of the kinetic mechanism provide insights on the functional role of the myosin Vc *in vivo*. In this section we will discuss these different kinetic features.

The maximal steady-state ATPase rate of MVc-S1 (1.8 s^{-1}) is markedly lower than that of chicken myosin Va (12 s^{-1}) (34) and *H. sapiens* myosin Vb (9.7 ± 0.4 s^{-1}) (31). Moreover, the apparent affinity of MVc-S1 to actin filaments (K_{ATPase}) is ~30-fold lower than chicken myosin Va (34) and 1.5-fold higher than that of myosin Vb (see Table 1). This lower actin affinity of MVc may be due in part to the difference in the loop 2 region, which has been shown to affect the K_{ATPase} of chicken myosin Va (27). Comparing the loop 2 of *H. sapiens* MVc to that of the *H. sapiens* myosin Va, the overall charge of MVc in this region is approximately half that of myosin Va (14). The *in vitro* actin gliding assays also reflected this phenomenon, whereby the velocity of filamentous actin translocation by eGFP-MVc-HMM was approximately an order of magnitude slower ($v_{Average}$ ~ 24 nm·s^{-1}) than myosin Va ($v_{Average}$ ~ 320 nm·s^{-1} (70) or myosin Vb ($v_{Average}$ ~ 220 nm·s^{-1} (31))). The *in vitro* actin gliding assays were also performed using the creatine phosphate/creatine phosphokinase ATP regeneration system to determine whether the levels of ADP contamination account for this slow velocity of actin filaments. Using the ATP regeneration system, the velocity of the actin filaments increased by approximately a factor of 2 (data not shown), to which is still reporting actin filaments velocity an order of magnitude slower than both myosins Va and Vb. Based on our transient kinetic measurements, we expected the actin gliding velocity of myosin Vc would be closer to that of myosins Va and Vb. The slower actin filament velocity may be accounted for by the hindrance because of weakly actin-bound heads of the eGFP-MVc-HMM.

Another possible reason for the slower *in vitro* actin gliding velocity of MVc may be due to the structure of the MVc lever arm or IQ motifs. The IQ motifs assembling the myosin Va lever have been shown to be separated by a repetition of 23 and 25 amino acid residues. However, the first two IQ motifs assembling the MVc lever seem to be separated by 23 and 28 amino acid residues (14). The different spacing of IQ motifs in the myosin Vc lever may contribute to the slow *in vitro* actin gliding velocities reported here as found previously with a mutant myosin Va construct where two alanine residues were inserted between the third and fourth IQ motifs (57). Both ensemble and single molecule studies of this myosin Va chimera showed slower velocity and smaller single displacements compared with the wild type construct without the additional alanines.

We note that the unexpectedly low *in vitro* actin gliding velocity of eGFP-MVc-HMM might possibly be due to a slow, rate-limiting isomerization between two actomyosin·ADP states that could occur after P_i release and precede ADP release. Such a step might remain undetected in the ADP release stopped-flow experiments if the "starting" state of the isomerization is an energetically unfavorable state that does not become populated upon ADP addition. However, the inability

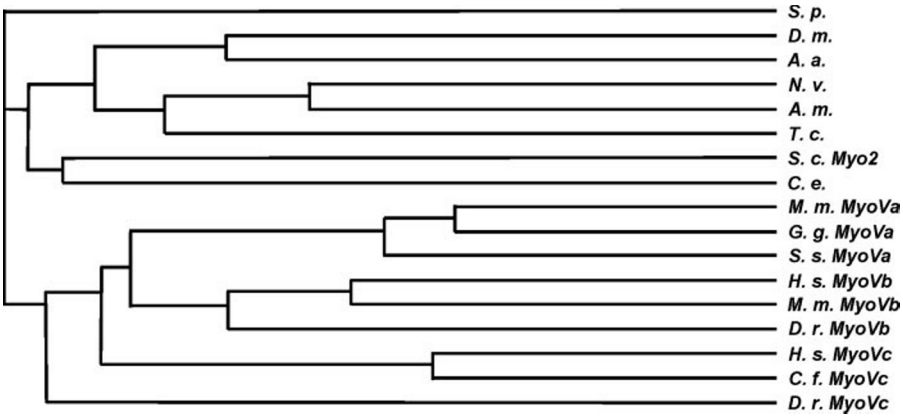

FIGURE 11. **Phylogenetic analysis of various myosin Vs from different organisms.** The consensus tree was generated using the ClustalW multiple sequence alignment program. The abbreviations used are as follows: *S. p., Strongylocentrotus purpuratus*; *D. m., Drosophila melanogaster*; *A. a., Aedes aegypti*; *N. v., Nagoni vetripennis*; *A. m., Apis mellifera*; *T. c., Triboleum castaneum*; *S. c., Saccharonyces cerevisiae*; *C. e., Caenorhabditis elegans*; *M. m., Mus musculus*; *G. g., Gallus gallus*; *S. s., Sus serofa*; *H. s., H. sapiens*; *D. r., Danio rerio*; *C. f., Canis familiaris*.

of eGFP-MVc-HMM to perform processive movement implies that its duty ratio is low, and thus the low actin gliding velocity results from hindrance by weakly actin-bound heads rather than an undetected strong actin-binding state.

Furthermore, both in the presence of nucleotide, as well as in the absence of nucleotide, myosin Vc seems to have a lower affinity to actin than myosin Va. The binding rate of MVc-S1 to actin in the absence of nucleotide is ~100-fold slower as compared with chicken myosin Va ($= 3\ \mu M^{-1}\cdot s^{-1}$ (34)). These rigor and nucleotide-bound on-rate constants may not be directly related to single molecule processivity. However, it may indirectly have implications on the actin on-rate constant in the weak actin-binding states, which parameter indeed is an important factor in processivity (*e.g.* a common factor determining strong and weak binding on-rate constants may be surface charge distribution). These implications may suggest that myosin Vc is inadequate for a single molecule cargo transporter.

Thus, for myosin Vc to function as a cargo transporter motor protein *in vivo*, it may function collectively as an ensemble of low duty ratio motors that can become a processive cargo transporter. However, myosin Vc may be useful for other cellular processes, such as budding, tethering, or fusion within the membrane trafficking system to which myosin Vc has been implicated (6, 14). The high affinity of myosin Vc for ADP may allow myosin Vc to have long lived, nonmoving attached states that may be a useful feature for a tension-generating, or anchoring, myosin *in vivo*.

Phylogenetic Analysis of H. sapiens Myosin Vc—A consensus tree of the *H. sapiens* myosin V isoforms (Va, Vb, and Vc) and *Drosophila* myosin V was reported recently (44), which indicated that the motor domain of the *H. sapiens* myosin Vc had a closer resemblance to the *Drosophila* myosin V than the other motor domains of the *H. sapiens* myosin V isoforms. Both *Drosophila* myosin V and the *H. sapiens* myosin Vc, as characterized in this study, are low duty ratio motors; however, the kinetic mechanisms of these two myosins are quite different. We therefore performed a more extensive phylogenetic analysis of the motor domain of myosin Vs from different organisms (Fig. 11). The result of the analysis indicated that the alignment of vertebrate myosin Vc in the consensus tree is separate from those of vertebrate myosin Va and Vb. Furthermore, all the vertebrate myosin Vs were located far from the *Drosophila* myosin V too. This result implies that the *H. sapiens* myosin Vc, even with the general dissimilarity of the kinetic cycle with its vertebrate myosin V counterparts, is closer to these isoforms than the *Drosophila* myosin V, which has a closer kinetic property to the *H. sapiens* myosin Vc. Perhaps evolution had evolved other vertebrate myosin V isoforms, Va and Vb, to become processive molecular motors.

High ADP Affinity of Myosin Vc—One unusual and intriguing aspect of the MVc-S1 actomyosin ATPase cycle is its high affinity for ADP. The ADP affinities were measured using the pyrene-actin fluorescence signal and the MANT-ADP signal, and independent experiments indicated similar results, suggesting that the ADP affinity (K_5') is higher for MVc-S1 (0.25–0.4 μM) than myosin Va (0.8 μM (34)) but not as high as the non-muscle myosin IIB (0.15 μM (54)). It may be that the myosin Vc is sensitive to ADP concentration changes and increases the duty ratio at high, or even at moderate, [ADP] as hypothesized previously for non-muscle myosin IIB (54). This unique feature may enhance the function of myosin Vc as a possible tension-generating molecular motor inside of a cell.

Future experiments are required to reveal if this is a plausible mechanism; however, this could be a novel *in vivo* process to alter a naturally occurring low duty ratio motor into a high duty ratio motor by functionally adapting to the physical environment they encounter, and it also may be a form of regulation for this molecular motor.

Acknowledgments—We thank Dr. Howard D. White for the generous gift of the MDCC-PBP; Dr. Takeshi Sakamoto for training to use the Olympus IX70 TIRF microscope system; Antoine F. Smith for rabbit muscle actin purification; Dr. J. R. Kuhn for the ImageJ plug-in; Dr. Fang Zhang for expert technical assistance; Rachel E. Farrow, Dr. Earl E. Homsher, and Dr. Attila Nagy for critical reading of the manuscript; and the members of the Laboratory of Molecular Physiology and Laboratory of Molecular Cardiology for support and critical advice.

Note Added in Proof—While this paper was under review, another report was published on the kinetics of human myosin Vc (Watanebe *et al.*, 2007) (71). They concluded, similar to our study, that the human myosin Vc is a low duty ratio, non-processive molecular motor; however, the details of the kinetic mechanism between the two studies are different.

REFERENCES

1. Richards, T. A., and Cavalier-Smith, T. (2005) *Nature* **436,** 1113–1118
2. Sellers, J. R. (1999) in *Myosins* (Ridley, A., and Frampton, J., eds), 2nd Ed., pp. 289–323, Oxford University Press, Oxford

3. Sellers, J. R. (2000) *Biochim. Biophys. Acta* **1496,** 3–22
4. Berg, J. S., Powell, B. C., and Cheney, R. E. (2001) *Mol. Biol. Cell* **12,** 780–794
5. DePina, A. S., and Langford, G. M. (1999) *Microsc. Res. Tech.* **47,** 93–106
6. Krendel, M., and Mooseker, M. S. (2005) *Physiol.* (*Bethesda*) **20,** 239–251
7. Brown, S. S. (1999) *Annu. Rev. Cell Dev. Biol.* **15,** 63–80
8. Reck-Peterson, S. L., Provance, D. W., Mooseker, M. S., and Mercer, J. A. (2000) *Biochim. Biophys. Acta* **1496,** 36–51
9. Wu, X. S., Rao, K., Zhang, H., Wang, F., Sellers, J. R., Matesic, L. E., Copeland, N. G., Jenkins, N. A., and Hammer, J. A., III (2002) *Nat. Cell Biol.* **4,** 271–278
10. Sweeney, H. L., and Houdusse, A. (2004) *Philos. Trans. R. Soc. Lond. B Biol. Sci.* **359,** 1829–1841
11. Sellers, J. R., and Veigel, C. (2006) *Curr. Opin. Cell Biol.* **18,** 68–73
12. Espreafico, E. M., Cheney, R. E., Matteoli, M., Nascimento, A. A. C., De Camilli, P. V., Larson, R. E., and Mooseker, M. S. (1992) *J. Cell Biol.* **119,** 1541–1557
13. Zhao, L. P., Koslovsky, J. S., Reinhard, J., Bahler, M., Witt, A. E., Provance, D. W., Jr., and Mercer, J. A. (1996) *Proc. Natl. Acad. Sci. U. S. A.* **93,** 10826–10831
14. Rodriguez, O. C., and Cheney, R. E. (2002) *J. Cell Sci.* **115,** 991–1004
15. Cheney, R. E., O'Shea, M. K., Heuser, J. E., Coelho, M. V., Wolenski, J. S., Espreafico, E. M., Forscher, P., Larson, R. E., and Mooseker, M. S. (1993) *Cell* **75,** 13–23
16. Mercer, J. A., Seperack, P. K., Strobel, M. C., Copeland, N. G., and Jenkins, N. A. (1991) *Nature* **349,** 709–713
17. Espindola, F. S., Espreafico, E. M., Coelho, M. V., Martins, A. R., Costa, F. R. C., Mooseker, M. S., and Larson, R. E. (1992) *J. Cell Biol.* **118,** 359–368
18. Provance, D. W., Jr., Wei, M., Ipe, V., and Mercer, J. A. (1996) *Proc. Natl. Acad. Sci. U. S. A.* **93,** 14554–14558
19. Wu, X., Bowers, B., Rao, K., Wei, Q., and Hammer, J. A., III (1998) *J. Cell Biol.* **143,** 1–20
20. Tuxworth, R. I., and Titus, M. A. (2000) *Traffic* **1,** 11–18
21. Westbroek, W., Lambert, J., Bahadoran, P., Busca, R., Herteleer, M. C., Smit, N., Mommaas, M., Ballotti, R., and Naeyaert, J. M. (2003) *J. Investig. Dermatol.* **120,** 465–475
22. Wilson, S. M., Yip, R., Swing, D. A., O'Sullivan, T. N., Zhang, Y., Novak, E. K., Swank, R. T., Russell, L. B., Copeland, N. G., and Jenkins, N. A. (2000) *Proc. Natl. Acad. Sci. U. S. A.* **97,** 7933–7938
23. Matesic, L. E., Yip, R., Reuss, A. E., Swing, D. A., O'Sullivan, T. N., Fletcher, C. F., Copeland, N. G., and Jenkins, N. A. (2001) *Proc. Natl. Acad. Sci. U. S. A.* **98,** 10238–10243
24. Libby, R. T., Lillo, C., Kitamoto, J., Williams, D. S., and Steel, K. P. (2004) *J. Cell Sci.* **117,** 4509–4515
25. Lapierre, L. A., Kumar, R., Hales, C. M., Navarre, J., Bhartur, S. G., Burnette, J. O., Provance, D. W., Jr., Mercer, J. A., Bahler, M., and Goldenring, J. R. (2001) *Mol. Biol. Cell* **12,** 1843–1857
26. Volpicelli, L. A., Lah, J. J., Fang, G., Goldenring, J. R., and Levey, A. I. (2002) *J. Neurosci.* **22,** 9776–9784
27. Swiatecka-Urban, A., Talebian, L., Kanno, E., Moreau-Marquis, S., Coutermarsh, B., Hansen, K., Karlson, K. H., Barnaby, R., Cheney, R. E., Langford, G. M., Fukuda, M., and Stanton, B. A. (2007) *J. Biol. Chem.* **282,** 23725–23736
28. Walker, M. L., Burgess, S. A., Sellers, J. R., Wang, F., Hammer, J. A., III, Trinick, J., and Knight, P. J. (2000) *Nature* **405,** 804–807
29. Burgess, S., Walker, M., Wang, F., Sellers, J. R., White, H. D., Knight, P. J., and Trinick, J. (2002) *J. Cell Biol.* **159,** 983–991
30. Coureux, P. D., Sweeney, H. L., and Houdusse, A. (2004) *EMBO J.* **23,** 4527–4537
31. Watanabe, S., Mabuchi, K., Ikebe, R., and Ikebe, M. (2006) *Biochemistry* **45,** 2729–2738
32. Nascimento, A. A., Cheney, R. E., Tauhata, S. B., Larson, R. E., and Mooseker, M. S. (1996) *J. Biol. Chem.* **271,** 17561–17569
33. Trybus, K. M., Krementsova, E., and Freyzon, Y. (1999) *J. Biol. Chem.* **274,** 27448–27456
34. De La Cruz, E. M., Wells, A. L., Rosenfeld, S. S., Ostap, E. M., and Sweeney, H. L. (1999) *Proc. Natl. Acad. Sci. U. S. A.* **96,** 13726–13731
35. De La Cruz, E. M., Sweeney, H. L., and Ostap, E. M. (2000) *Biophys. J.* **79,** 1524–1529
36. Wang, F., Chen, L., Arcucci, O., Harvey, E. V., Bowers, B., Xu, Y., Hammer, J. A., III, and Sellers, J. R. (2000) *J. Biol. Chem.* **275,** 4329–4335
37. Yengo, C. M., De La Cruz, E. M., Safer, D., Ostap, E. M., and Sweeney, H. L. (2002) *Biochemistry* **41,** 8508–8517
38. Yengo, C. M., and Sweeney, H. L. (2004) *Biochemistry* **43,** 2605–2612
39. De La Cruz, E. M., and Ostap, E. M. (2004) *Curr. Opin. Cell Biol.* **16,** 61–67
40. Mehta, A. D., Rock, R. S., Ridf, M., Spudich, J. A., Mooseker, M. S., and Cheney, R. E. (1999) *Nature* **400,** 590–593
41. Sakamoto, T., Amitani, I., Yokota, E., and Ando, T. (2000) *Biochem. Biophys. Res. Commun.* **272,** 586–590
42. Forkey, J. N., Quinlan, M. E., Shaw, M. A., Corrie, J. E., and Goldman, Y. E. (2003) *Nature* **422,** 399–404
43. Yildiz, A., Forkey, J. N., McKinney, S. A., Ha, T., Goldman, Y. E., and Selvin, P. R. (2003) *Science* **300,** 2061–2065
44. Toth, J., Kovacs, M., Wang, F., Nyitray, L., and Sellers, J. R. (2005) *J. Biol. Chem.* **280,** 30594–30603
45. Kovacs, M., Wang, F., Hu, A., Zhang, Y., and Sellers, J. R. (2003) *J. Biol. Chem.* **278,** 38132–38140
46. Yang, Y., Kovacs, M., Xu, E., Anderson, J. B., and Sellers, J. R. (2005) *J. Biol. Chem.* **280,** 32061–32068
47. Spudich, J. A., and Watt, S. (1971) *J. Biol. Chem.* **246,** 4866–4871
48. Pollard, T. D. (1984) *J. Cell Biol.* **99,** 769–777
49. Houk, T. W., Jr., and Ue, K. (1974) *Anal. Biochem.* **62,** 66–74
50. Ishijima, A., Kojima, H., Funatsu, T., Tokunaga, M., Higuchi, H., Tanaka, H., and Yanagida, T. (1998) *Cell* **92,** 161–171
51. Takagi, Y., Homsher, E. E., Goldman, Y. E., and Shuman, H. (2006) *Biophys. J.* **90,** 1295–1307
52. Brune, M., Hunter, J. L., Corrie, J. E. T., and Webb, M. R. (1994) *Biochemistry* **33,** 8262–8271
53. Trentham, D. R., Bardsley, R. G., Eccleston, J. F., and Weeds, A. G. (1972) *Biochem. J.* **126,** 635–644
54. Wang, F., Kovacs, M., Hu, A. H., Limouze, J., Harvey, E. V., and Sellers, J. R. (2003) *J. Biol. Chem.* **278,** 27439–27448
55. Brune, M., Corrie, J. E., and Webb, M. R. (2001) *Biochemistry* **40,** 5087–5094
56. Kovacs, M., Wang, F., and Sellers, J. R. (2005) *J. Biol. Chem.* **280,** 15071–15083
57. Sakamoto, T., Wang, F., Schmitz, S., Xu, Y. H., Xu, Q., Molloy, J. E., Veigel, C., and Sellers, J. R. (2003) *J. Biol. Chem.* **278,** 29201–29207
58. Kuhn, J. R., and Pollard, T. D. (2005) *Biophys. J.* **88,** 1387–1402
59. Ostap, E. M., and Pollard, T. D. (1996) *J. Cell Biol.* **132,** 1053–1060
60. White, H. D., Belknap, B., and Webb, M. R. (1997) *Biochemistry* **36,** 11828–11836
61. Snyder, G. E., Sakamoto, T., Hammer, J. A., III, Sellers, J. R., and Selvin, P. R. (2004) *Biophys. J.* **87,** 1776–1783
62. Sakamoto, T., Yildiz, A., Selvin, P. R., and Sellers, J. R. (2005) *Biochemistry* **44,** 16203–16210
63. Geeves, M. A. (1991) *Biochem. J.* **274,** 1–14
64. Coluccio, L. M., and Geeves, M. A. (1999) *J. Biol. Chem.* **274,** 21575–21580
65. El Mezgueldi, M., Tang, N., Rosenfeld, S. S., and Ostap, E. M. (2002) *J. Biol. Chem.* **277,** 21514–21521
66. De La Cruz, E. M., Ostap, E. M., and Sweeney, H. L. (2001) *J. Biol. Chem.* **276,** 32373–32381
67. Dawson, M. J., Gadian, D. G., and Wilkie, D. R. (1978) *Nature* **274,** 861–866
68. Kushmerick, M. J., Moerland, T. S., and Wiseman, R. W. (1992) *Proc. Natl. Acad. Sci. U. S. A.* **89,** 7521–7525
69. Radda, G. K. (1986) *Science* **233,** 640–645
70. Homma, K., Saito, J., Ikebe, R., and Ikebe, M. (2000) *J. Biol. Chem.* **275,** 34766–34771
71. Watanabe, S., Watanabe, T., Sato, O., Awata, J., Homma, K., Umeki, N., Higuchi, H., Ikebe, R., and Ikebe, M. (December 12, 2007) *J. Biol. Chem.* 10.1074/jbc.M707657200